Cohesin still drives homologous recombination repair of DNA double-strand breaks in late mitosis.

Jessel Ayra-Plasencia[1,2,#,*], Lorraine Symington[3], and Félix Machín[1,2,4,*]

[1] Hospital Universitario Nuestra Señora de Candelaria, 38010 Santa Cruz De Tenerife, Spain.

[2] Instituto de Tecnologías Biomédicas, Universidad de La Laguna, 38200 San Cristóbal de La Laguna, Spain.

[3] Department of Microbiology and Immunology, Columbia University Medical Center, New York, United States.

[4] Facultad de Ciencias de la Salud, Universidad Fernando Pessoa Canarias, Las Palmas de Gran Canaria, Spain.

[#] Present address: Unidad de Investigación, Hospital Universitario de Canarias, 38320 San Cristóbal de La Laguna, Spain

* Co-corresponding authors: jessel.ayra.plasencia@gmail.com; fmachin@fciisc.es

Abstract

The cohesin complex maintains sister chromatid cohesion from S phase to anaphase onset. Cohesin also plays roles in chromosome structure and DNA repair. At anaphase onset, the cohesin subunit Scc1 is cleaved to allow segregation in an orderly manner, although some residual cohesin subunits remain to maintain chromosome structure. Efficient DNA double-strand break (DSB) repair by homologous recombination (HR) with the sister chromatid also depends on cohesin. Here, we have tested whether residual cohesin is important during DSB repair in anaphase/telophase (late mitosis). Using the well-established MAT switching system, we first show that HR is molecularly functional in late mitosis, and then show that cohesin is required for its efficiency. During DSBs in late mitosis, the segregated sister loci get closer and have episodes of coalescence, which may favour repair by HR. Here, we also show that these cytological phenotypes also depend on cohesin. Finally, full-length Scc1 returns after DSBs in late mitosis, suggesting that *de novo* widespread cohesin complexes can support these retrograde behaviours.

Keywords

DNA double-strand break; anaphase; telophase; cohesin; homologous recombination

Introduction

Cell survival and genome integrity depend on the faithful segregation of chromosomes in anaphase. From the S phase until the anaphase onset, the highly conserved cohesin complex plays an essential role in the structural maintenance of sister chromatids. Cohesin is a multiprotein complex composed in yeast of Smc1, Smc3, Scc1 (also known as Mcd1), Scc3 and Pds5 subunits (Hirano, 2000; Michaelis *et al*., 1997; Sjögren and Nasmyth, 2001). At the core of the complex, Smc1, Smc3 and Scc1 form a heterotrimeric ring that embraces and holds the replicated sister chromatids together and well-aligned until reaching G_2/M (Díaz-Martínez *et al*., 2008; Koshland and Guacci, 2000; Laloraya *et al*., 2000; Michaelis *et al*., 1997; Strunnikov *et al*., 1993). Cohesin subunits are loaded onto chromosomes in G_1 by the Scc2-Scc3 complex (Ciosk *et al*., 2000). When cells enter S phase, the acetyl-transferase Eco1 acetylates Smc3, which inhibits the ATPase activity of Smc1-Smc3 heads and prevents the opening of the Smc3-Scc1 interface (Çamdere *et al*., 2015; Chan *et al*., 2012; Huber *et al*., 2016; Murayama and Uhlmann, 2015; Ström *et al*., 2007; Unal *et al*., 2007). This embraces the nascent sister chromatids and establishes cohesion (Uhlmann and Nasmyth, 1998). Once sister chromatids are ready for segregation, the APC^{Cdc20} (Anaphase Promoting Complex associated with its regulatory cofactor Cdc20) initiates anaphase by degrading securin/Pds1, so that the separase/Esp1 becomes active. Separase then cleaves the Scc1 subunit by proteolysis, releasing sister chromatids from cohesion (Cohen-Fix *et al*., 1996; Michaelis *et al*., 1997; Nasmyth and Haering, 2009; Uhlmann *et al*., 1999; Yamamoto *et al*., 1996). The fragmented Scc1 is then rapidly degraded (Rao *et al*., 2001), while a pool of Smc1-Smc3 dimers appears to remain through anaphase (Renshaw *et al*., 2010; Tanaka *et al*., 1999). This pool however becomes loose as Smc3 is deacetylated by Hos1 in anaphase (Chan *et al*., 2012; Huber *et al*., 2016; Murayama and Uhlmann, 2015). Interestingly, some cohesin-dependent cohesion remains at chromosome arms during anaphase, suggesting that residual cohesin is present despite separase activation (Renshaw *et al*., 2010).

In addition to its role in sister chromatid cohesion, cohesin has also been involved in chromosome structure and DNA repair. On the one hand, cohesin can hold two DNA segments within the same chromatin forming an extruded loop (Lazar-Stefanita *et al*., 2017; Schalbetter *et al*., 2017). On the other hand, DNA double strand breaks (DSBs) produce the so-called damage-induced cohesion (DI-cohesion) (Kim *et al*., 2010). Following DNA damage, cohesin is recruited and accumulated both along 50 – 100 kb surrounding the DSB site and genome-wide (Ström *et al*., 2004; Ünal *et al*., 2004). The cohesin recruitment creates a firm anchoring of two well-aligned sister chromatids, which in turn facilitates DSB repair by homologous recombination (HR) (Hou *et al*., 2022; Phipps and Dubrana, 2022). In this regard, DNA damage kinases such as Mec1 and Chk1 phosphorylate Scc1 to initiate the cohesion establishment in post-replicative cells (Heidinger-Pauli *et al*., 2008).

HR is a DSB repair mechanism that uses a homologous template for restoring the original broken DNA. HR is highly reliable when the correct template is used, which in mitotic cells is the sister chromatid. Hence, HR is the preferred repair mechanism from S to G_2/M, when the sister chromatid is available in close proximity (Langerak and Russell, 2011; Mathiasen and

72 Lisby, 2014; Symington *et al*., 2014). Before DNA replication, in G_1, the alternative error-
73 prone non-homologous end joining (NHEJ) is used instead. Cells coordinate the choice of
74 either NHEJ or HR based on the activity of cyclin dependent kinase (CDK). Low CDK keeps
75 cells in G_1 and favours NHEJ, whereas high CDK is present in S and G_2/M and activates HR.

76 Noticeably, there is a paradox in his link between high CDK and HR. In the cell cycle
77 window that spans from anaphase to the telophase-to-G_1 transition (we will refer to this window
78 as late mitosis), high CDK is set to favour HR despite a sister chromatid is not in proximity
79 (Machín and Ayra-Plasencia, 2020). In a previous study, we showed that sister loci can indeed
80 move closer and coalesce and that HR still appears important for DSB survival in late mitosis
81 (Ayra-Plasencia and Machín, 2019). Considering these observations, a second paradox arises,
82 how can sister loci coalesce and HR be that important in the absence of cohesin? We have
83 addressed such a paradox here.

84 **Results and Discussion**

85 **The HO-mediated DSB is resected efficiently in late mitosis.**

86 In a previous report, we showed from both genetic and cytological points of view that HR
87 was still active in late mitosis. In this work, we applied molecular methods to determine
88 whether HR can occur in late mitosis. To this aim, we followed the DSB processing and repair
89 of a single DSB generated by the inducible HO endonuclease, which cuts the HO cutting site
90 (*HOcs*) at the *MAT* locus in chromosome III. The DSB was generated once cells were arrested
91 in late mitosis (late anaphase/telophase) through the thermosensitive *cdc15-2* allele. Cdc15 is
92 a mitotic kinase that drives telophase-to-G_1 transition (Machín and Ayra-Plasencia, 2020).

93 We first tested whether the HO-induced DSB is efficiently resected into 3' ssDNA tails in
94 late mitosis. Resection is necessary to form the protruding 3' nucleofilaments that invade the
95 donor homologous sequence to restore the break by HR (Peng *et al*., 2021; Symington, 2016).
96 To confirm and quantitate the formation of ssDNA flanking the *HOcs*, we used a qPCR
97 approach whereby primers can only amplify a target DNA cut with the restriction enzyme *StyI*
98 if it has been rendered single-stranded by resection (Fig 1a, b) (Gnügge *et al*., 2018; Zierhut
99 and Diffley, 2008). We used a strain carrying deletions for the *HML* and *HMR* loci, the two
100 ectopic homologous templates for HR with the *MAT* locus. In this manner, the normal HR flow
101 from resection to invasion is blocked, which boosts ssDNA detection. For the controlled
102 induction of the HO endonuclease, we ectopically introduced the encoding gene under the
103 control of a promoter that responds to β-estradiol (Gnügge and Symington, 2020). Two
104 different locations downstream of the *HOcs* were monitored to determine both the initial
105 resection (0.7 Kb from *HOcs*) and the kinetics further away (5.7 Kb). In addition, cells arrested
106 in either G_2/M (Nz) or late mitosis (*cdc15-2*) were directly compared to each other. Cells were
107 first arrested for 3 h, the HO was induced afterwards, and samples were taken every hour during
108 a 4 h time course while sustaining the HO induction (Fig 1c). As expected, cells in G_2/M
109 efficiently resected the *HOcs* DSB. The time to reach half of the maximum possible resection
110 ($t_{1/2}$) was ~1 h at 0.7 Kb and ~2.5 h at 5.7 Kb from the DSB, respectively. Resection in late

111 mitosis was only slightly delayed at 0.7 Kb (t1/2 ~1.5 h), whereas the delay was more
112 pronounced at 5.7 Kb ($t_{1/2}$ ~ 3.5 h). Overall, resection in late mitosis appears almost as efficient
113 as in G_2/M. The slight delay may be due to either the fact that CDK activity in late mitosis
114 (though still high) is slightly inferior to that at G_2/M, or the different conditions of arrests (Nz
115 at 25 ºC *vs*. just 34 ºC). Together with the samples for the qPCR, samples for Western blot of
116 Rad53 were taken. Rad53 is an effector kinase of the DNA Damage Checkpoint (DDC) that
117 gets activated by hyperphosphorylation after being recruited to the 3' ssDNA overhands
118 (Branzei and Foiani, 2006). In agreement with the resection profile (Fig 1c), Rad53
119 hyperphosphorylation also occurred in late mitosis, although with ~1 h delay (Fig 1d).

120 **HR can still switch the *MAT* locus in late mitosis.**

121 Once resection begins, cells are normally committed to recombine because long ssDNA
122 fragments do not work as efficient substrates for NHEJ. In our haploid strain, HR at the *MAT*
123 locus after the HO-driven DSB implies the gene conversion from the *MAT*a to the *MAT*α allele,
124 whereas repair by NHEJ results in reconstitution of the *MAT*a allele (Fig 2a) (Yamaguchi and
125 Haber, 2021). This gene conversion can be detected by Southern blot because of a restriction
126 fragment length polymorphism for *StyI*. Cells that are in G_1 can barely repair the *HOcs* DSB,
127 whereas those in G_2/M do so through HR (Ira *et al*., 2004). To check whether HR was efficient
128 at the *HOcs* DSB in late mitosis, we performed an experimental setup similar to the one shown
129 above, but with two important differences. On the one hand, the strain bears the wild type *HML*
130 locus, so that HR can be completed if it is called upon; and on the other hand, a just a pulse of
131 HO induction was applied (1 h with β-estradiol only), so that there is room for the complete
132 repair of all generated DSBs. Samples were taken at the time of the arrest, after the pulse, and
133 all through the repair window. We confirmed by Western blot that HO (HO tagged with the
134 Flag epitope in this case) is produced after the pulse, and rapidly degraded afterwards (Fig 2b,
135 HO-Flag blot). Likewise, Rad53 hyperphosphorylation confirmed that the *HOcs* DSB has been
136 correctly sensed (Fig 2b, Rad53 blot). The Southern blot showed that **(i)** most *MAT*a locus in
137 the cell population has been efficiently cut after the HO pulse (Fig 2c and d; decrease of the
138 *MAT*a band intensity and rise of that of the HO cut); and **(ii)** most DSBs are repaired afterwards
139 exclusively through HR (Fig 2c and d; drop of the HO cut band intensity and rise of that of the
140 *MAT*α). No signs of DSB by NHEJ were observed (the remaining *MAT*a band stays constant
141 throughout).

142 Overall, we concluded that HR is the chosen repair pathway in late mitosis. This is in
143 agreement with predictions based on CDK activity and also fits well with the genetic and
144 cytological data we have obtained before (Ayra-Plasencia and Machín, 2019; Machín and
145 Ayra-Plasencia, 2020). By contrast, this emphasizes the paradoxes of having HR in the context
146 of mostly segregated sister chromatids and without the cohesin complex holding them together.
147 The first paradox was at least partly solved in our previous report as we observed that sister
148 loci can rejoin after DSBs (Ayra-Plasencia and Machín, 2019). We have now explored the
149 second paradox further as DI-cohesion appears important for efficient DSB repair by HR (Hou
150 *et al*., 2022; Phipps and Dubrana, 2022).

151 **The MAT switching in late mitosis depends on cohesin.**

152 Smc1 and Smc3 subunits remain attached to chromatin after segregation (Garcia-Luis *et al*.,
153 2022; Renshaw *et al*., 2010; Tanaka *et al*., 1999). In cells arrested in *cdc15-2*, the Smc1-Smc3
154 pool mostly resides at centromeres where it brings together adjacent regions in both
155 chromosome arms (Garcia-Luis *et al*., 2022). Of note, this configuration could favour the
156 physical interaction of the *MAT* and the *HML* loci, which may in turn promote a rapid and
157 efficient HR-driven MAT switching. Thus, we tested whether MAT switching was dependent
158 on this residual centromeric cohesin. To this aim, we tagged the Smc3 subunit with the auxin-
159 mediated degron system (aid*) in the strain that expresses HO from the β-estradiol promoter.

160 To check that the system was functional, a serial dilution spot assay was carried out (Fig.
161 3a). The strain expressing Smc3-aid* was plated on YPDA and YPDA plus 8 mM of the auxin
162 indole-acetic acid (IAA). Alongside, we also plated a derivative where we had removed the
163 preceptive F-box protein OsTIR1, which forms the functional ubiquitin ligase responsible for
164 targeting the aid* for degradation upon IAA addition (Morawska and Ulrich, 2013). Since
165 cohesin is an essential complex for vegetative growth, the lack of growth in the *SMC3-AID**
166 *OsTIR1* strain strongly points out that Smc3-aid* is degraded efficiently.

167 Next, we used this strain to degrade Smc3 after cells have been arrested in late mitosis and
168 before the HO-mediated DSB (Fig. 3b-d). In our experimental setup, a pool of Smc3 was
169 clearly present at the *cdc15-2* arrest (Fig. 3b). This pool was acetylated at lysine residues K112
170 and K113, further suggesting that it is chromatin-bound (Rolef Ben-Shahar *et al*., 2008; Unal
171 *et al*., 2008). After IAA addition, there was a clear decline in Smc3-aid* levels. After 1 h in
172 IAA, a 1 h pulse of HO expression was triggered, which allowed us to follow both DSB
173 generation and its subsequent repair without residual cohesin (Fig. 3c,d). More than 90% of the
174 Smc3-aid* had disappeared by the time the HO promoter was shut down.

175 Contrary to what is seen in the wild type, the Smc3 absence drastically delayed gene conversion
176 from *MAT*a to *MAT*α (Fig. 3c,d). Even though the cut efficiency without Smc3 is lower than in
177 the wild type (~50 % *vs*. ~70 %, respectively), wild type cells performed HR with ~80 %
178 efficiency (considering the HO cut band as 100 %), whereas Smc3-depleted cells only repaired
179 to *MAT*α in ~35 %. Also, the detection of DNA damage through Rad53 phosphorylation seems
180 fainter and slightly delayed (Fig. 3b). Of note, It was previously reported that cohesin was not
181 that important for the MAT switching in G_2/M-arrested cells, despite it being essential for
182 efficient post-replicative DSB repair (Ünal *et al*., 2004). One possible explanation for the
183 discrepancy with our MAT switching results may reside in the different experimental setup,
184 i.e. auxin-induced degradation of Smc3 versus Scc1 inactivation using a thermosensitive allele.
185 Alternatively, the Smc1-Smc3 dimer by itself could be sufficient for cohesin-dependent DSB
186 repair. Finally, DI-cohesion in G_2/M is, perhaps, not such important for bringing the *MAT* and
187 *HML* locus together since sister chromatids can rely on other cohesin-independent linkages,
188 such as catenations; a scenario that might not be present in late mitosis.

189

190 **Scc1 becomes stable after DSBs in late mitosis.**

191 At the anaphase onset, the separase/Esp1 cleaves Scc1, opening the cohesin ring and
192 releasing sister chromatids from cohesion. Thereafter, Scc1 needs to be translated *de novo* since
193 cleaved fragments are unstable and degraded by the proteasome (Rao *et al*., 2001). However,
194 it is known that activation of Esp1 can be blocked by DDC kinases (Yam *et al*., 2020). In
195 addition, DDC kinases also phosphorylate Scc1 to facilitate DI-cohesion at a post-replicative
196 stage (Heidinger-Pauli *et al*., 2008). Thus, it is feasible that DSB generation in late mitosis can
197 stabilize *de novo* Scc1 as well as rendering it cohesive.

198 To know how Scc1 behaves after DSBs in late mitosis, a strain unable to repair the HO-
199 mediated DSB at the *MAT* locus (Δ*hml* Δ*hmr* double mutant) but bearing Scc1 tagged with
200 three tandem copies of the *myc* epitope was first blocked in telophase at 34 ºC for 3 hours.
201 Then, the culture was divided into three. The first one served as a mock control, whereas the
202 others were used to generate a single (2 µM β-estradiol) and multiple (10 µg · mL^{-1} phleomycin)
203 DSBs. Incubation of subcultures was prolonged at 34 ºC for 2 extra hours. The presence or
204 absence of Scc1-3myc was then checked by Western blot. As expected, Scc1 band was detected
205 for both cycling cells and those blocked in G_2/M. The Scc1 signal disappeared almost entirely
206 when cells were arrested in late mitosis and remained low in the mock control two hours later.
207 Surprisingly, full-length Scc1 was restored after single and multiple DSBs generation (Fig. 4a).
208 This finding suggests that the cohesin complex could be newly formed and loaded onto the
209 breaks, promoting the DI-cohesion and easing the recombinational coalescent events.

210 **Sister loci approximation and coalescence after DSBs in late mitosis also depend on**
211 **cohesin.**

212 Considering the above results on Smc3-dependent HR and Scc1 reappearing after DSBs
213 in late mitosis, we next studied whether cohesin was needed for the remarkable phenotypes we
214 described before under the microscope. The most striking phenotype was the partial regression
215 of sister chromatid segregation, which included back migration and coalescence of sister loci
216 in a single cell body of the dividing cell (Ayra-Plasencia and Machín, 2019). To this aim, the
217 same strain we used before for these studies was transformed to obtain Smc3-aid*. The strain
218 carries several *tetO* sequences at the telomeric region of the right arm of chromosome XII
219 (cXIIr-Tel), as well as the TetR-YFP as the fluorescent reporter for both sister telomeres. The
220 cXIIr-Tel is the last to segregate in anaphase (Machín *et al*., 2005); hence, back migration and
221 coalescence of these sister loci are bona fide signs of regressed anaphase (Ayra-Plasencia and
222 Machín, 2019). Cells arrested in late mitosis were submitted to Smc3 degradation and
223 subsequent generation of DSBs as above. Again, Western blot analyses showed that cells
224 degraded ~ 80 % of Smc3 after 1 hour in IAA, and subsequent generation of DSBs with
225 phleomycin triggered Smc3-independent Rad53 phosphorylation at similar levels than the
226 control without IAA, positioning any cohesin role downstream of the DDC (Fig. 4b). Cells that
227 were not treated with IAA but were having DSBs reverted segregation of cXIIr-Tel in ~ 13 %
228 of the telophase-blocked cells [$p<0.0001$ relative to categories quantified at the arrest] (Fig.
229 4c). As we found before (Ayra-Plasencia and Machín, 2019), ~ 7 % of cells showed two foci

230 in the same cellular body (i.e. back migration), whereas ~ 6 % had coalescence events. In
231 contrast, cells deficient for Smc3 did not show a significant statistical difference from the mock
232 non-DSB situation. This result supports that the cohesin complex is at least essential to promote
233 the passing of chromosomes across the bud neck, which results in back migration and is a
234 prerequisite for the subsequent coalescence.

235 Conclusions

236 In this work we have addressed whether HR was molecularly efficient in yeast cells arrested
237 in late mitosis. We have used the well-established MAT switching system and found that HR
238 is indeed working in late mitosis, complementing previous results that pointed in this direction
239 both genetically and cytologically (Ayra-Plasencia and Machín, 2019). In addition, we have
240 addressed that paradox of having HR in a cell mitotic stage with no sister chromatid cohesion.
241 Our results suggest not only that residual cohesin, or at least residual Smc1-Smc3 dimers, play
242 a role in an efficient HR at the *MAT* locus, but also that the partial regression of the anaphase
243 we cytologically observed before is dependent on cohesin. The fact that Scc1, the cohesin
244 subunit that is cleaved and degraded at the anaphase onset, returns in late mitosis after DSB
245 generation, suggests that *de novo* cohesion could be established, perhaps globally. This new
246 cohesin may favour repair by HR with the intact sister of DSBs generated in such a late cell
247 cycle stage. Further research will be needed to confirm whether cohesion is re-established in
248 late mitosis upon DNA damage as well as its whereabouts and consequences for late
249 segregation after DSB repair.

250 Material and Methods

251 Strains and experimental conditions.

252 The table 1 contains the *S. cerevisiae* strains used in this work. Genetic backgrounds are
253 either W303 or YPH499. Strain construction was either performed by lithium acetate-based
254 transformation on pre-made frozen competent cells, either by crosses and sporulation (Knop *et*
255 *al*., 1999).

256 **Table 1. Strains used in this work.**

Strain	Relevant Genotype[1]	Origin
FM588	(YPH499) *MATa ura3-52 lys2-801 ade2-101 trp1-Δ63 his3-Δ200 leu2-Δ1 bar1-Δ; ade2-101::TetR:YFP::ADE2; tetO(5.6Kb)::1061Kb-ChrXII::HIS3; cdc15-2:9myc::Hph*	F. Machín lab
LSY4319-1C	(W303) *MATα leu2-3,112 trp1-1 can1-100 ura3-1 ade2-1 his3-11,15 RAD5 Δhml Δhmr*; *leu2-3::lexO4p:HO:FLAG:CYC1t::ACT1p:LexA-ER-B112-T:CYC1p::LEU2MX* (pRG646)	L. Symington lab

FM2450	LSY4319-1C; *cdc15-2:9myc::Hph*	This work
FM2520	FM2450; *SCC1:3myc::HIS3MX*	This work
FM2531	FM588; *HMLα Δhmr::HIS3MX; leu2-3::lexO4p:HO:FLAG:CYC1t::ACT1p:LexA-ER-B112-T:CYC1p::LEU2MX*	This work
FM2672	FM2531; *SMC3:AID*:9myc::KanMX*	This work
FM2680	FM2672; *ura3-52::ADH1p:OsTIR1:9myc::URA3*	This work
FM2626	FM588; *SMC3:AID*:9myc::KanMX*	This work
FM2628	FM2626; *ura3-52::ADH1p:OsTIR1:9myc::URA3*	This work

[1] Semicolons separate genetic modifications obtained through sequential transformation steps. Intermediate strains are omitted.

Strains were cultured overnight in the YPD medium (10 $g \cdot L^{-1}$ yeast extract, 20 $g \cdot L^{-1}$ peptone and 20 $g \cdot L^{-1}$ glucose) with moderate shaking (180 rpm). The day after, 10-100 µL of grown cells were diluted into a flask containing an appropriate YPD volume and grown overnight at 25 ºC again. Finally, the exponentially growing culture was adjusted to OD_{600} = 0.5 to start the experiment.

In general, cells were first arrested in late mitosis by incubating the culture at 34 ºC for 3 hours (all strains carry the *cdc15-2* thermosensitive allele). Then, the culture was split in two, one subculture remained untreated (mock), and DSBs were generated in the second one. When a G_2/M arrest was required, 15 $\mu g \cdot mL^{-1}$ nocodazole (Nz; Sigma-Aldrich, M1404) was added to the asynchronous culture, which was then incubated at 25°C for 3 h (with a 7.5 $\mu g \cdot mL^{-1}$ Nz shot at 2 h). To conditionally degrade the Smc3-aid* variant, 8 mM of the auxin 3-indol-acetic acid (IAA; Sigma-Aldrich, I2886) was added to the arrested cells 1 h prior to generating DSBs.

DSB generation was accomplished by incubating the culture for 1 to 3 hours with either 10 $\mu g \cdot mL^{-1}$ phleomycin (random DSBs) or 2 µM of β-estradiol (HO-driven DSBs). For the *HOcs* DSB, the corresponding strain harbours an integrative system based on a β-estradiol inducible promoter (Ottoz *et al*., 2014). These strains were constructed by transforming with the pRG464 plasmid (Gnügge and Symington, 2020).

qPCR for DSB resection.

In the resection experiments, qPCR was performed on genomic DNA (gDNA) extracted by the glass beads/phenol method (Hoffman and Winston, 1987). Experimental details on the resection assay can be found in (Gnügge *et al*., 2018). Briefly, each gDNA sample was divided into two and one aliquot was digested with *StyI*-HF (NEB, R3500S). Then, qPCR reactions were mounted using the PowerUp™ SYBR™ Green Master Mix (Thermo Scientific, A25741)

282 and run in a BioRad CFX384 Real-Time PCR instrument (10 µl final volume in 384-well block
283 plates).

284 Resection was calculated as a normalized fraction ($f_{resected}$) to that of the HOcs effectively
285 cut by HO (f). These two parameters were calculated by their corresponding formulas (Gnügge
286 *et al*., 2018).

287 **Western blot for protein levels and phosphorylation**

288 Western blotting was performed as reported before (Ayra-Plasencia and Machín, 2019). The
289 trichloroacetic acid TCA method was used for protein extraction. Total protein was quantified
290 in a Qubit 4 Fluorometer (Thermo Fisher Scientific, Q33227). Proteins were resolved in 7.5%
291 SDS-PAGE gels and transferred to PVFD membranes (Pall Corporation, PVM020C099). The
292 membrane was stained with Ponceau-S solution (PanReac AppliChem, A2935) as a loading
293 reference. The following primary antibodies were used for immunoblotting: mouse monoclonal
294 α-HA (1:1,000; Sigma-Aldrich, H9658); mouse monoclonal α-myc (1: 5,000; Sigma-Aldrich,
295 M4439); mouse monoclonal α-Pgk1 (1:5,000; Thermo Fisher Scientific, 22C5D8), and mouse
296 monoclonal α-miniaid (1:500; MBL, M214-3). The secondary antibody was a horseradish
297 peroxidase polyclonal goat anti-mouse (from 1:5,000 to 1:10,000, depending on the primary
298 antibody; Promega, W4021). Proteins were detected with the ECL chemiluminescence reagent
299 (GE Healthcare, RPN2232), and visualized in a Vilber-Lourmat Fusion Solo S chamber.

300 **Southern blot for the MAT switching assay.**

301 In this case, gDNA was extracted by digesting with 50U lyticase (Sigma-Aldrich, L4025) a
302 cell pellet previously resuspended in 200 µl of digestion buffer (1 % SDS, 100 mM NaCl, 50
303 mM Tris-HCl, and 10 mM EDTA). Then, the gDNA was phase separated by
304 phenol:chloroform (PanReac AppliChem, A0944), precipitated with ethanol, resuspended in
305 TE 1X with 10 $\mu g \cdot mL^{-1}$ RNase A, precipitated again, and resuspended in TE 1X. Then, the
306 gDNA was digested with *StyI*-HF, the restriction fragments separated on a 1.2% low EEOO
307 LS Agarose gel, and finally Southern blotted. Southern blot was carried out by a saline
308 downwards transference onto a positively charged nylon membrane (Hybond-N+, Amersham-
309 GE; RPN303B) (García-Luis and Machín, 2014). DNA probes against *ACT1* and *MAT* loci
310 were made using Fluorescein-12-dUTP Solution (ThermoFisher; R0101) and the Expand™
311 High Fidelity PCR System (Roche; 11732641001). Hybridization with fluorescein-labelled
312 probes was performed overnight at 68°C. The following day, the membrane was incubated with
313 an anti-fluorescein antibody coupled to alkaline phosphatase (Roche; 11426338910), and the
314 chemiluminescent signal detected using CDP-star (Amersham; RPN3682). Blots were
315 visualized in a Vilber-Lourmat Fusion Solo S chamber.

316 For band quantification, each individual band was normalized to the ACT1 signal in the
317 lane. Then, a second normalization to the MATa band at the arrest was performed.

318

319 **Data representation and statistics.**

320 Three types of graphs were used to represent the data: bar charts, marker line graphs and
321 box plots. In box plots, the center line represents the medians, box limits represent the 25th and
322 75th percentile, the whiskers extend to the 5th and 95th percentiles, and the dots represent
323 outliers. Error bars in all bar and line charts represent the standard error of the mean (sem) of
324 three independent biological replicates. Individual values are also represented as dots in the bar
325 charts. Graphpad Prism 9 was used for generating the charts and for statistical analysis.
326 Differences between experimental data points were generally estimated using the Mann-
327 Whitney U test for box plots and two-way ANOVA with Tukey post hoc for bar charts.

328 **Acknowledgements**

329 We would like to thank other members from Machín's and Symington's labs for enriching
330 and fruitful discussion. This work was supported by the Spanish Ministry of Science and
331 Innovation (research grants BFU2017-83954-R and PID2021-123716OB-I00 to F.M.). Both
332 grants were co-financed with the FSE structural funds. This work was also supported by the
333 National Institute of Health (research grant NIH R35 GM126997 to L.S.).

334 **Author contributions**

335 **J Ayra-Plasencia**: Performed all experiments in this work; constructed all strains; prepared
336 the corresponding figures; gave critical insights as to the direction and development of the
337 study; and co-wrote the manuscript.

338 **L Symington**: Results shown in Figures 1 and 2 were generated in her lab; hosted J.A-P. during
339 the generation of these results; gave critical insights as to the direction and development of the
340 study; and was responsible for funding acquisition and project administration.

341 **F Machín**: Results shown in Figures 3 and 4 were generated in his lab; was the supervisor of
342 J.A-P.; gave critical insights as to the direction and development of the study; was responsible
343 for funding acquisition and project administration; and co-wrote the manuscript.

344 **References**

345 Ayra-Plasencia J, Machín F. 2019. DNA double-strand breaks in telophase lead to
346 coalescence between segregated sister chromatid loci. *Nat Commun* **10**:2862.
347 doi:10.1038/s41467-019-10742-8

348 Branzei D, Foiani M. 2006. The Rad53 signal transduction pathway: Replication fork
349 stabilization, DNA repair, and adaptation. *Exp Cell Res* **312**:2654–9.
350 doi:10.1016/j.yexcr.2006.06.012

351 Çamdere G, Guacci V, Stricklin J, Koshland D. 2015. The ATPases of cohesin interface with
352 regulators to modulate cohesin-mediated DNA tethering. *Elife* **4**.

353 doi:10.7554/eLife.11315

354 Chan K-L, Roig MB, Hu B, Beckouët F, Metson J, Nasmyth K. 2012. Cohesin's DNA Exit
355 Gate Is Distinct from Its Entrance Gate and Is Regulated by Acetylation. *Cell* **150**:961–
356 974. doi:10.1016/j.cell.2012.07.028

357 Ciosk R, Shirayama M, Shevchenko Anna, Tanaka T, Toth A, Shevchenko Andrej, Nasmyth
358 K. 2000. Cohesin's binding to chromosomes depends on a separate complex consisting
359 of Scc2 and Scc4 proteins. *Mol Cell* **5**:243–254. doi:10.1016/S1097-2765(00)80420-7

360 Cohen-Fix O, Peters JM, Kirschner MW, Koshland D. 1996. Anaphase initiation in
361 Saccharomyces cerevisiae is controlled by the APC-dependent degradation of the
362 anaphase inhibitor Pds1p. *Genes Dev* **10**:3081–93. doi:10.1101/GAD.10.24.3081

363 Díaz-Martínez L a, Giménez-Abián JF, Clarke DJ. 2008. Chromosome cohesion - rings,
364 knots, orcs and fellowship. *J Cell Sci* **121**:2107–14. doi:10.1242/jcs.029132

365 Garcia-Luis J, Bordelet H, Thierry A, Koszul R, Aragon L. 2022. Depletion or cleavage of
366 cohesin during anaphase differentially affects chromatin structure and segregation. *Elife*
367 **11**:1–22. doi:10.7554/eLife.80147

368 García-Luis J, Machín F. 2014. Mus81-Mms4 and Yen1 resolve a novel anaphase bridge
369 formed by noncanonical Holliday junctions. *Nat Commun* **5**:5652.
370 doi:10.1038/ncomms6652

371 Gnügge R, Symington LS. Efficient DNA double-strand break formation at single or multiple
372 defined sites in the Saccharomyces cerevisiae genome. Nucleic Acids Res. 2020 Nov
373 18;48(20):e115. doi: 10.1093/nar/gkaa833

374 Gnügge R, Oh J, Symington LS. 2018. Processing of DNA Double-Strand Breaks in Yeast.
375 *Methods Enzymol* **600**:1–24. doi:10.1016/bs.mie.2017.11.007

376 Heidinger-Pauli JM, Ünal E, Guacci V, Koshland D. 2008. The Kleisin Subunit of Cohesin
377 Dictates Damage-Induced Cohesion. *Mol Cell* **31**:47–56.
378 doi:10.1016/j.molcel.2008.06.005

379 Hirano T. 2000. Chromosome cohesion, condensation, and separation. *Annu Rev Biochem*
380 **69**:115–44. doi:10.1146/annurev.biochem.69.1.115

381 Hoffman CS, Winston F. 1987. A ten-minute DNA preparation from yeast efficiently releases
382 autonomous plasmids for transformaion of Escherichia coli. *Gene* **57**:267–272.
383 doi:10.1016/0378-1119(87)90131-4

384 Hou W, Li Y, Zhang J, Xia Y, Wang X, Chen H, Lou H. 2022. Cohesin in DNA damage
385 response and double-strand break repair. *Crit Rev Biochem Mol Biol* **57**:333–350.
386 doi:10.1080/10409238.2022.2027336

387 Huber RG, Kulemzina I, Ang K, Chavda AP, Suranthran S, Teh J-T, Kenanov D, Liu G,
388 Rancati G, Szmyd R, Kaldis P, Bond PJ, Ivanov D. 2016. Impairing Cohesin Smc1/3
389 Head Engagement Compensates for the Lack of Eco1 Function. *Structure* **24**:1991–
390 1999. doi:10.1016/j.str.2016.09.001

391 Ira G, Pellicioli A, Balijja A, Wang X, Fiorani S, Carotenuto W, Liberi G, Bressan D, Wan L,
392 Hollingsworth NM, Haber JE, Foiani M. 2004. DNA end resection, homologous
393 recombination and DNA damage checkpoint activation require CDK1. *Nature*
394 **431**:1011–7. doi:10.1038/nature02964

395 Kim B-J, Li Yehua, Zhang J, Xi Y, Li Yumei, Yang T, Jung SY, Pan X, Chen R, Li W, Wang
396 Y, Qin J. 2010. Genome-wide Reinforcement of Cohesin Binding at Pre-existing
397 Cohesin Sites in Response to Ionizing Radiation in Human Cells. *J Biol Chem*
398 **285**:22784–22792. doi:10.1074/jbc.M110.134577

399 Knop M, Siegers K, Pereira G, Zachariae W, Winsor B, Nasmyth K, Schiebel E. 1999.
400 Epitope tagging of yeast genes using a PCR-based strategy: more tags and improved
401 practical routines. *Yeast* **15**:963–72. doi:10.1002/(SICI)1097-
402 0061(199907)15:10B<963::AID-YEA399>3.0.CO;2-W

403 Koshland DE, Guacci V. 2000. Sister chromatid cohesion: the beginning of a long and
404 beautiful relationship. *Curr Opin Cell Biol* **12**:297–301. doi:10.1016/s0955-
405 0674(00)00092-2

406 Laloraya S, Guacci V, Koshland D. 2000. Chromosomal addresses of the cohesin component
407 Mcd1p. *J Cell Biol* **151**:1047–56. doi:10.1083/JCB.151.5.1047

408 Langerak P, Russell P. 2011. Regulatory networks integrating cell cycle control with DNA
409 damage checkpoints and double-strand break repair. *Philos Trans R Soc Lond B Biol Sci*
410 **366**:3562–71. doi:10.1098/rstb.2011.0070

411 Lazar-Stefanita L, Scolari VF, Mercy G, Muller H, Guérin TM, Thierry A, Mozziconacci J,
412 Koszul R. 2017. Cohesins and condensins orchestrate the 4D dynamics of yeast
413 chromosomes during the cell cycle. *EMBO J* **36**:2684–2697.
414 doi:10.15252/embj.201797342

415 Machín F, Ayra-Plasencia J. 2020. Are Anaphase Events Really Irreversible? The Endmost
416 Stages of Cell Division and the Paradox of the DNA Double-Strand Break Repair.
417 *BioEssays* **42**:2000021. doi:10.1002/bies.202000021

418 Machín F, Torres-Rosell J, Jarmuz A, Aragón L. 2005. Spindle-independent condensation-
419 mediated segregation of yeast ribosomal DNA in late anaphase. *J Cell Biol* **168**:209–19.
420 doi:10.1083/jcb.200408087

421 Mathiasen DP, Lisby M. 2014. Cell cycle regulation of homologous recombination in
422 Saccharomyces cerevisiae. *FEMS Microbiol Rev* **38**:172–184. doi:10.1111/1574-
423 6976.12066

424 Michaelis C, Ciosk R, Nasmyth K. 1997. Cohesins: Chromosomal proteins that prevent
425 premature separation of sister chromatids. *Cell* **91**:35–45. doi:10.1016/S0092-
426 8674(01)80007-6

427 Morawska M, Ulrich HD. 2013. An expanded tool kit for the auxin-inducible degron system
428 in budding yeast. *Yeast* **30**:341–51. doi:10.1002/yea.2967

429 Murayama Y, Uhlmann F. 2015. DNA Entry into and Exit out of the Cohesin Ring by an
430 Interlocking Gate Mechanism. *Cell* **163**:1628–1640. doi:10.1016/j.cell.2015.11.030

431 Nasmyth K, Haering CH. 2009. Cohesin: Its Roles and Mechanisms. *Annu Rev Genet*
432 **43**:525–558. doi:10.1146/annurev-genet-102108-134233

433 Ottoz DSM, Rudolf F, Stelling J. 2014. Inducible, tightly regulated and growth condition-
434 independent transcription factor in Saccharomyces cerevisiae. *Nucleic Acids Res* **42**.
435 doi:10.1093/nar/gku616

436 Peng H, Zhang S, Chen X. 2021. Monitoring 5'-End Resection at Site-Specific Double-
437 Strand Breaks by Southern Blot Analysis. *Methods Mol Biol* **2196**:245–255.
438 doi:10.1007/978-1-0716-0868-5_20

439 Phipps J, Dubrana K. 2022. DNA Repair in Space and Time: Safeguarding the Genome with
440 the Cohesin Complex. *Genes (Basel)* **13**. doi:10.3390/genes13020198

441 Rao H, Uhlmann F, Nasmyth K, Varshavsky A. 2001. Degradation of a cohesin subunit by
442 the N-end rule pathway is essential for chromosome stability. *Nature* **410**:955–9.
443 doi:10.1038/35073627

444 Renshaw MJ, Ward JJ, Kanemaki M, Natsume K, Nédélec FJ, Tanaka TU. 2010. Condensins
445 promote chromosome recoiling during early anaphase to complete sister chromatid
446 separation. *Dev Cell* **19**:232–44. doi:10.1016/j.devcel.2010.07.013

447 Rolef Ben-Shahar T, Heeger S, Lehane C, East P, Flynn H, Skehel M, Uhlmann F. 2008.
448 Eco1-dependent cohesin acetylation during establishment of sister chromatid cohesion.
449 *Science* **321**:563–6. doi:10.1126/science.1157774

450 Schalbetter SA, Goloborodko A, Fudenberg G, Belton J-M, Miles C, Yu M, Dekker J, Mirny
451 L, Baxter J. 2017. SMC complexes differentially compact mitotic chromosomes
452 according to genomic context. *Nat Cell Biol* **19**:1071–1080. doi:10.1038/ncb3594

453 Sjögren C, Nasmyth K. 2001. Sister chromatid cohesion is required for postreplicative
454 double-strand break repair in Saccharomyces cerevisiae. *Curr Biol* **11**:991–5.
455 doi:10.1016/s0960-9822(01)00271-8

456 Ström L, Karlsson C, Lindroos HB, Wedahl S, Katou Y, Shirahige K, Sjögren C. 2007.
457 Postreplicative formation of cohesion is required for repair and induced by a single
458 DNA break. *Science* **317**:242–5. doi:10.1126/science.1140649

459 Ström L, Lindroos HB, Shirahige K, Sjögren C. 2004. Postreplicative Recruitment of
460 Cohesin to Double-Strand Breaks Is Required for DNA Repair. *Mol Cell* **16**:1003–1015.
461 doi:10.1016/j.molcel.2004.11.026

462 Strunnikov A V., Larionov VL, Koshland D. 1993. SMC1: an essential yeast gene encoding a
463 putative head-rod-tail protein is required for nuclear division and defines a new
464 ubiquitous protein family. *J Cell Biol* **123**:1635–48. doi:10.1083/jcb.123.6.1635

465 Symington LS. 2016. Mechanism and regulation of DNA end resection in eukaryotes. *Crit*
466 *Rev Biochem Mol Biol* **51**:195–212. doi:10.3109/10409238.2016.1172552

467 Symington LS, Rothstein R, Lisby M. 2014. Mechanisms and Regulation of Mitotic
468 Recombination in Saccharomyces cerevisiae. *Genetics* **198**:795–835.
469 doi:10.1534/genetics.114.166140

470 Tanaka T, Cosma MP, Wirth K, Nasmyth K. 1999. Identification of cohesin association sites
471 at centromeres and along chromosome arms. *Cell* **98**:847–858. doi:10.1016/S0092-
472 8674(00)81518-4

473 Uhlmann F, Lottspeich F, Nasmyth K. 1999. Sister-chromatid separation at anaphase onset is
474 promoted by cleavage of the cohesin subunit Scc1. *Nature* **400**:37–42.
475 doi:10.1038/21831

476 Uhlmann F, Nasmyth K. 1998. Cohesion between sister chromatids must be established
477 during DNA replication. *Curr Biol* **8**:1095–101. doi:10.1016/s0960-9822(98)70463-4

478 Ünal E, Arbel-Eden A, Sattler U, Shroff R, Lichten M, Haber JE, Koshland D. 2004. DNA
479 Damage Response Pathway Uses Histone Modification to Assemble a Double-Strand
480 Break-Specific Cohesin Domain. *Mol Cell* **16**:991–1002.
481 doi:10.1016/j.molcel.2004.11.027

482 Unal E, Heidinger-Pauli JM, Kim W, Guacci V, Onn I, Gygi SP, Koshland DE. 2008. A
483 molecular determinant for the establishment of sister chromatid cohesion. *Science*
484 **321**:566–9. doi:10.1126/science.1157880

485 Unal E, Heidinger-Pauli JM, Koshland D. 2007. DNA double-strand breaks trigger genome-
486 wide sister-chromatid cohesion through Eco1 (Ctf7). *Science* **317**:245–8.
487 doi:10.1126/science.1140637

488 Yam CQX, Chia DB, Shi I, Lim HH, Surana U. 2020. Dun1, a Chk2-related kinase, is the
489 central regulator of securin-separase dynamics during DNA damage signaling. *Nucleic*
490 *Acids Res* **48**:6092–6107. doi:10.1093/nar/gkaa355

491 Yamaguchi M, Haber JE. 2021. Monitoring Gene Conversion in Budding Yeast by Southern
492 Blot Analysis. *Methods Mol Biol* **2153**:221–238. doi:10.1007/978-1-0716-0644-5_16

493 Yamamoto A, Guacci V, Koshland D. 1996. Pds1p is required for faithful execution of
494 anaphase in the yeast, Saccharomyces cerevisiae. *J Cell Biol* **133**:85–97.
495 doi:10.1083/jcb.133.1.85

496 Zierhut C, Diffley JFX. 2008. Break dosage, cell cycle stage and DNA replication influence
497 DNA double strand break response. *EMBO J* **27**:1875–85. doi:10.1038/emboj.2008.111

498

499

500 **FIGURE LEGENDS**

501 **Figure 1. Resection in late mitosis is almost as efficient as in G_2/M.** (**a**) Schematic
502 representation of the HO resection assay. Primers (blue arrows) are designed to amplify a
503 sequence that contains a *StyI* target site adjacent to the HO cutting site (*HOcs*). When this
504 restriction enzyme is used on the extracted genomic DNA, amplification is inhibited. If
505 resection extends beyond the *StyI* site, StyI does not cut and the primers can amplify. (**b**)
506 Summary table of the amplification yield obtained after the *StyI* digestion for each situation
507 (mock control *vs*. HO induction). (**c**) Charts depicting the resection kinetics for two different
508 amplicons located at 726 bp and 5.7 kb downstream the *HOcs* break (mean ± sem, n=3; $f_{resected}$
509 is the proportion of resected DNA. (**d**) Representative Western blots against Rad53 to follow
510 the sensing of DNA damage detection in G_2/M versus late mitosis.

511 **Figure 2. Yeast cells use HR to repair the HO DSB in late mitosis.** (**a**) Schematic of the
512 fragments obtained after a *StyI* digestion for both *MAT*a and *MAT*α sequences. The probe to
513 detect the fragments by Southern blot is in blue. When the *MAT*a locus is intact, the digestion
514 gives rise to a 0.9 kb fragment. The HO cutting site (*HOcs*) is located within the *StyI*-digested
515 *MAT*a locus. Thus, the HO-driven DSB shortens the fragment to 0.7 kb. HR leads to a gene
516 conversion to *MAT*α, which results in the loss of a *StyI* restriction site and a new fragment of
517 1.8 kb. (**b-d**) Cells were first blocked in the *cdc15-2* arrest at 34 ºC for 3 hours (Tel). Then, the
518 HO-mediated DSB was generated by adding 2 µM β-estradiol. After 1 hour, the β-estradiol
519 was washed away, and samples were taken to monitor the repair for 3 hours. (**b**) Representative
520 Western blot analyses for HO induction and subsequent degradation (tagged with Flag epitope)
521 and the DSB sensing through Rad53 hyperphosphorylation. A PGK1 western blot served as a
522 housekeeping and Ponceau-S staining of the membrane as a loading control for all lanes. The
523 leftmost lane in the Ponceau-S corresponds to the protein weight marker. (**c**) Representative
524 Southern blot for the MAT switching assay in late mitosis. Alongside the MAT probe, a second
525 probe against the *ACT1* gene (1.1 kb fragment) was included for normalization. The MAT
526 probe also recognizes an allele-independent MAT distal fragment (2.2 kb). (**d**) Quantification
527 of relative band intensities in the MAT switching Southern blots (mean ± sem, n=3). Individual
528 values were normalized to the *ACT1* signals. Then, every lane was normalized to *MAT*a at the
529 arrest. Tel: Telophase. +β-E: β-estradiol addition.

530 **Figure 3. Smc3 degradation delays HR at the *MAT* locus in late mitosis.** (**a**) Serial dilution
531 spot assay for the *SMC3:AID** derivative of the strain used in Figure 2. The effect of Smc3-
532 aid* degradation was tested in the presence of 8 mM IAA. The same strain without the
533 ubiquitin-ligase *OsTIR1* was also used as the control. (**b-d**) Cells were treated as in Figure 2
534 but including a 1 h IAA step between the *cdc15-2* arrest and the induction of HO. IAA was
535 then maintained throughout the experiment. (**b**) Representative Western blot as in Figure 2b
536 but also including Smc3-aid* decline after IAA addition. (**b**) Representative Southern blot for
537 the MAT switching assay after degrading Smc3-aid* in late mitosis. (**d**) Quantification of
538 relative band intensities for MAT switching Southern blots (mean ± sem, n=3). Values were
539 normalized as in Figure 2d. The MAT switching in the wild type strain is represented alongside
540 for comparison. Tel: Telophase. +β-E: β-estradiol addition. +IAA: Indole-acetic acid.

541 **Figure 4. Scc1 returns after DSBs in late mitosis and the absence of Smc3 inhibits sister**
542 **telomere coalescence.** (**a**) Western blot against Scc1-3myc (detected with an α-myc antibody).
543 This experiment compares Scc1-3myc levels in an asynchronous, G_2/M- and telophase-blocked
544 cultures. Cells arrested in telophase were further subdivided into three subcultures and treated
545 as indicated for another two hours (mock, phleomycin, and HO endonuclease). The leftmost
546 lane is a control strain for Scc1 without the 3myc epitope tag. PGK1 protein served as a
547 housekeeping. Ponceau-S staining is also shown as a loading control. Asyn.: Asynchronous.
548 Tel: Telophase. +Phle: 10 $mg \cdot mL^{-1}$ phleomycin. +HO: 2 μM β-estradiol. *: Unspecific band
549 detected by the α-myc antibody just over the Scc1-3myc signal. (**b, c**) A *SMC3:AID** strain
550 that reports the segregation status of the chromosome XII right telomere (cXIIr-Tel) was used
551 for this regressed anaphase assay. Cells arrested in late mitosis were divided into two. One
552 subculture was treated with 8 mM IAA for 1 h. Then, each subculture was, in turn, divided into
553 two, one serving as a mock control and the other was treated with 10 $\mu g \cdot mL^{-1}$ phleomycin for
554 an extra hour. Samples were taken at the indicated time points for Western blotting and
555 microscopy. (**b**) Representative Western blot. Smc3-aid* was monitored using an anti-mini-
556 AID monoclonal antibody. Rad53 hyperphosphorylation was also monitored as a control to
557 confirm DNA damage after phleomycin addition. PGK1 was used as the housekeeping control
558 to quantify the remaining Smc3 signal. Ponceau-S staining of the membrane is also shown as
559 a loading reference for each lane. (**c**) Chart representing quantifications of sister telomere
560 segregation status (mean ± sem, n=3). Cells were classified into three categories depending on
561 cXIIr-Tel location within the elongated nucleus: (i) Segregated, showing two foci well
562 separated in distinct cell bodies; (ii) same body, presenting both sister telomeres in one of the
563 daughter-to-be cells; and (iii) coalescence, only one cXIIr-Tel focus. Statistical significance
564 was calculated through 2-way ANOVA and multiple comparisons analysis. IAA: Indole-acetic
565 acid; Tel: Telophase (i.e. late mitosis); ns: non-significant statistical difference.

Figure 1

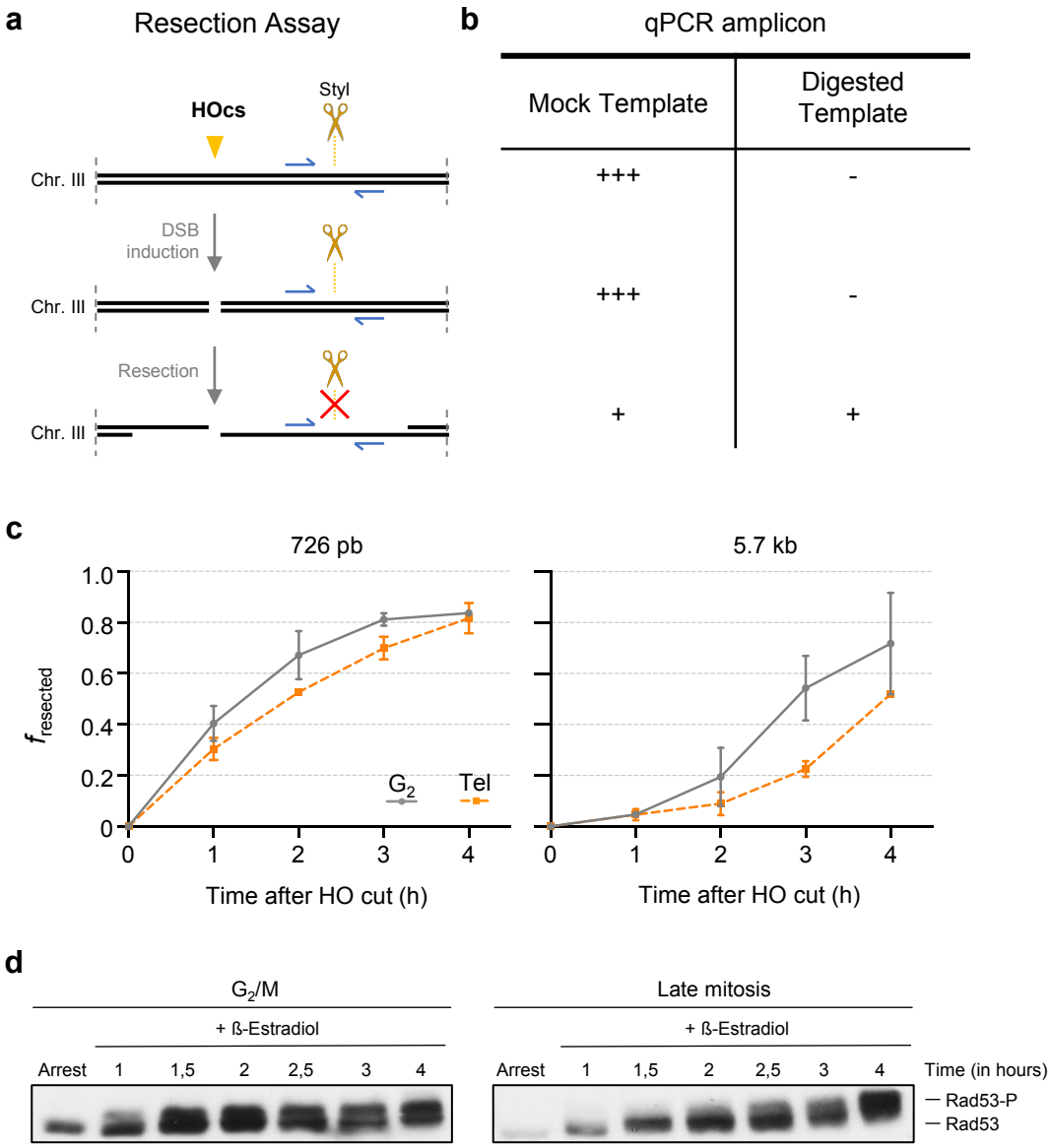
a
Resection Assay
HOcs
SfiI
Chr. III
DSB induction
Chr. III
Resection
Chr. III
b
qPCR amplicon
Mock Template
Digested Template
+++
-
+++
-
+
+
c
726 pb
5.7 kb
$f_{resected}$
1.0
0.8
0.6
0.4
0.2
0
G2
Tel
0
1
2
3
4
Time after HO cut (h)
Time after HO cut (h)
d
G2/M
Late mitosis
+ ß-Estradiol
+ ß-Estradiol
Arrest
1
1,5
2
2,5
3
4
Arrest
1
1,5
2
2,5
3
4
Time (in hours)
Rad53-P
Rad53

Figure 2

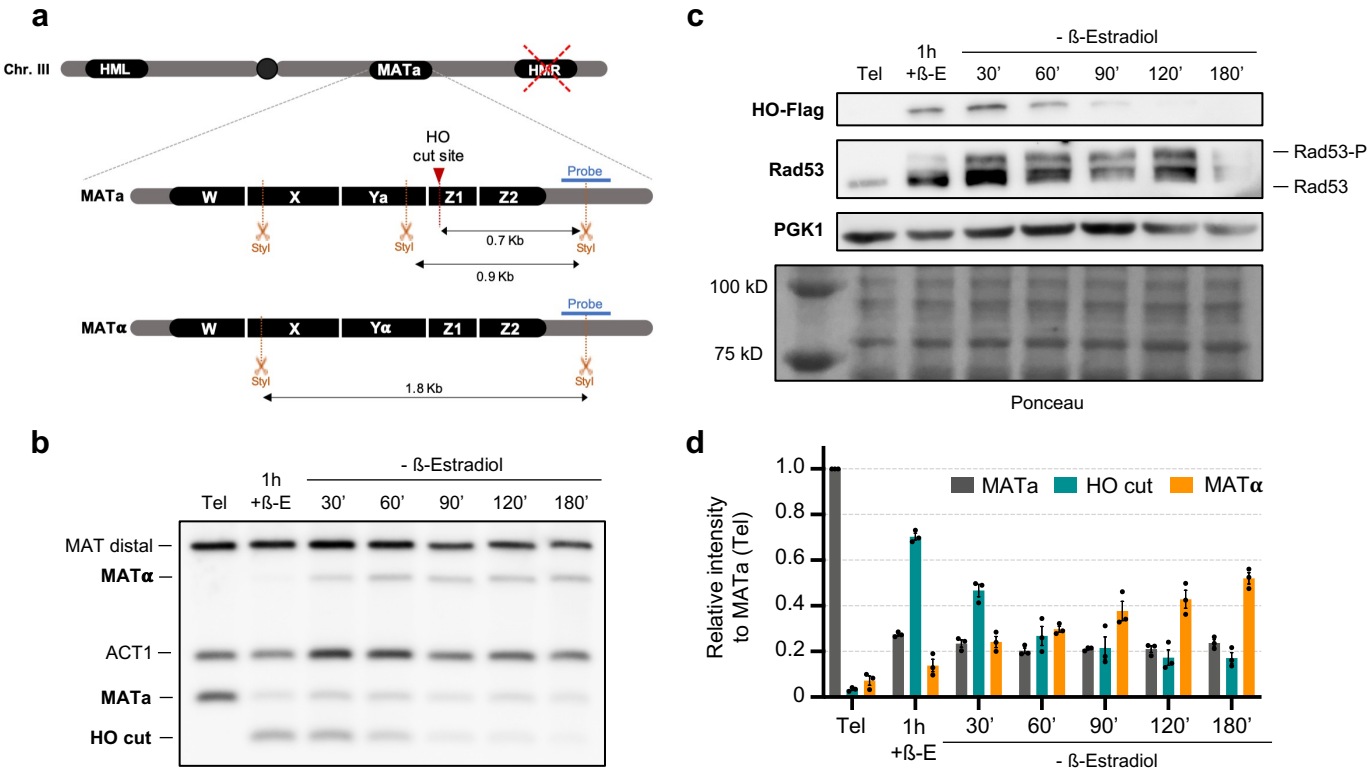
a
Chr. III
HML
MATa
HMR
HO
cut site
Probe
MATa
W
X
Ya
Z1
Z2
StyI
StyI
StyI
0.7 Kb
0.9 Kb
Probe
MATα
W
X
Yα
Z1
Z2
StyI
StyI
1.8 Kb
b
- ß-Estradiol
Tel
1h
+ß-E
30'
60'
90'
120'
180'
MAT distal
MATα
ACT1
MATa
HO cut
c
- ß-Estradiol
Tel
1h
+ß-E
30'
60'
90'
120'
180'
HO-Flag
Rad53
Rad53-P
Rad53
PGK1
100 kD
75 kD
Ponceau
d
MATa
HO cut
MATα
Relative intensity
to MATa (Tel)
1.0
0.8
0.6
0.4
0.2
0
Tel
1h
+ß-E
30'
60'
90'
120'
180'
- ß-Estradiol

Figure 3

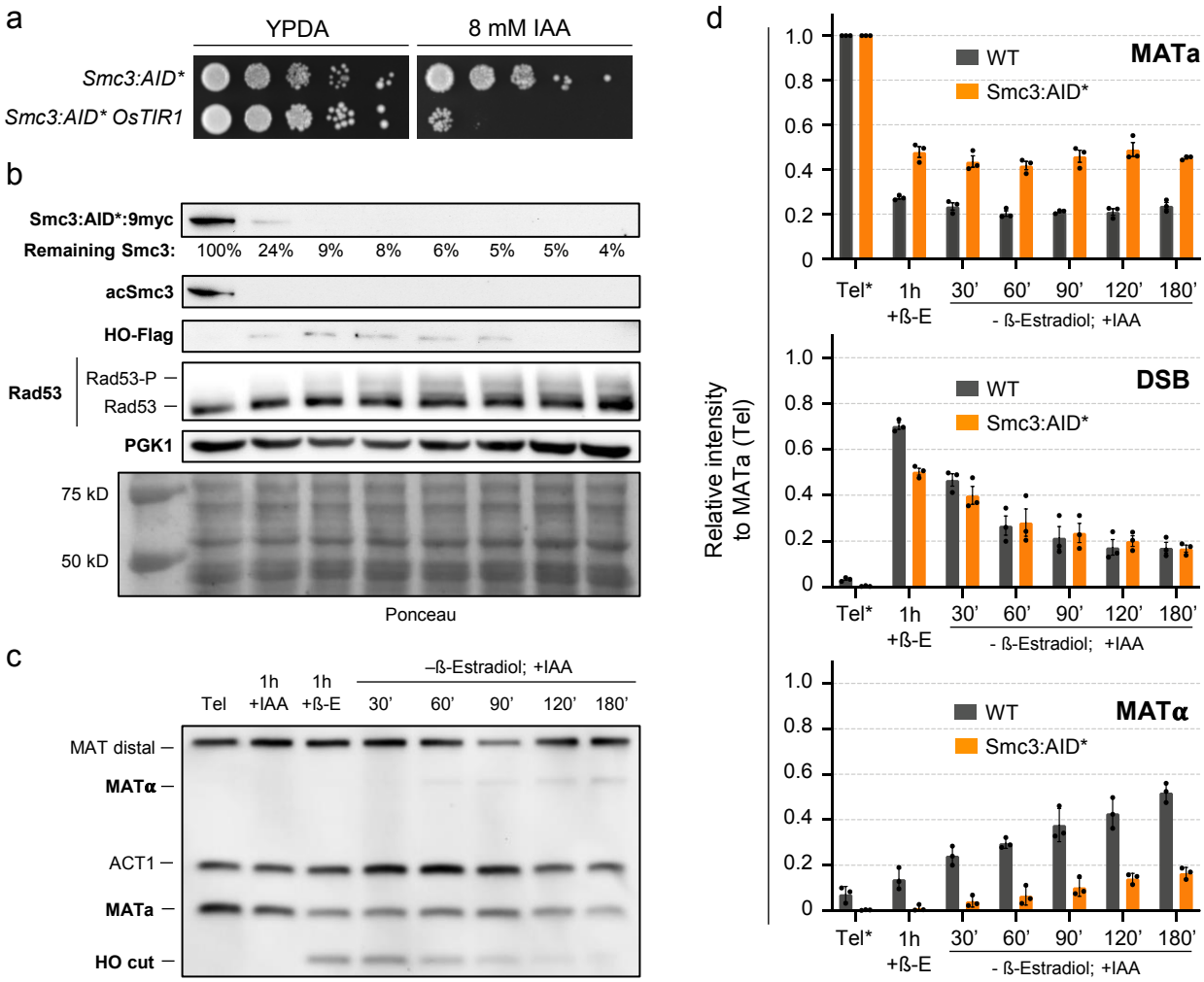
a
YPDA
8 mM IAA
Smc3:AID*
Smc3:AID* OsTIR1
b
Smc3:AID*:9myc
Remaining Smc3:
100%
24%
9%
8%
6%
5%
5%
4%
acSmc3
HO-Flag
Rad53
Rad53-P
Rad53
PGK1
75 kD
50 kD
Ponceau
c
–ß-Estradiol; +IAA
Tel
1h +IAA
1h +ß-E
30'
60'
90'
120'
180'
MAT distal
MATα
ACT1
MATa
HO cut
d
Relative intensity to MATa (Tel)
WT
Smc3:AID*
MATa
DSB
MATα
Tel*
1h +ß-E
- ß-Estradiol; +IAA

Figure 4

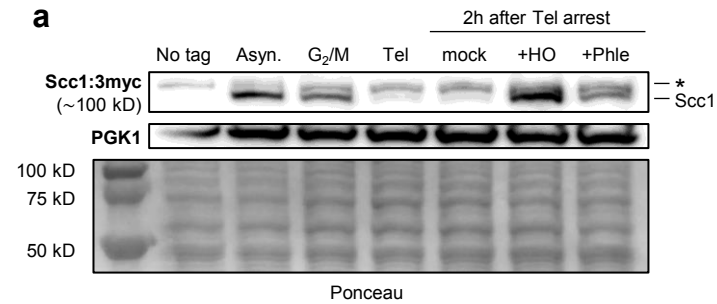
a
2h after Tel arrest
No tag
Asyn.
G2/M
Tel
mock
+HO
+Phle
Scc1:3myc
(~100 kD)
*
Scc1
PGK1
100 kD
75 kD
50 kD
Ponceau

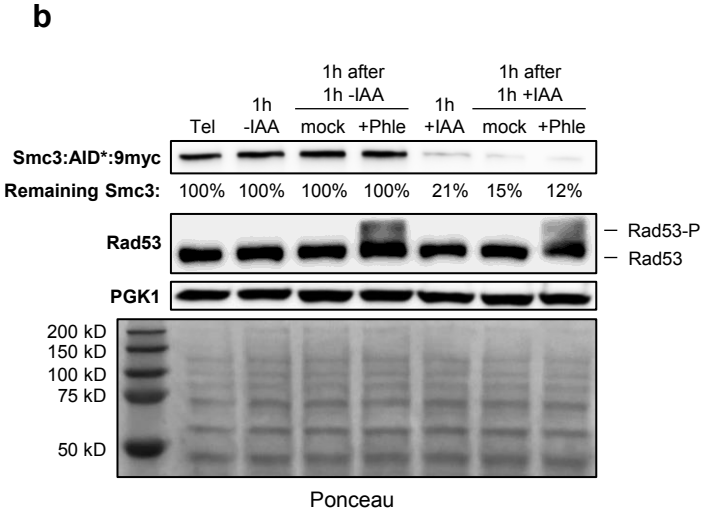
b
1h after
1h -IAA
1h after
1h +IAA
Tel
1h
-IAA
mock
+Phle
1h
+IAA
mock
+Phle
Smc3:AID*:9myc
Remaining Smc3:
100%
100%
100%
100%
21%
15%
12%
Rad53
Rad53-P
Rad53
PGK1
200 kD
150 kD
100 kD
75 kD
50 kD
Ponceau

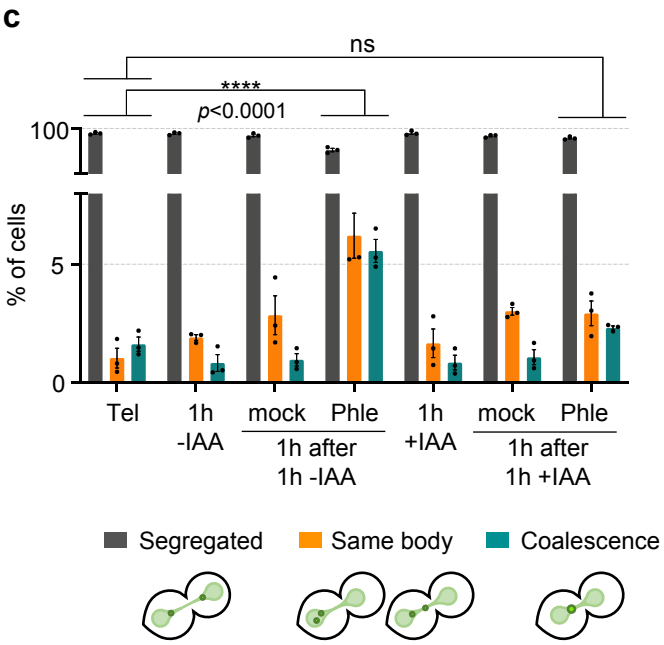
c
ns
****
p<0.0001
100
5
0
% of cells
Tel
1h
-IAA
mock
Phle
1h after
1h -IAA
1h
+IAA
mock
Phle
1h after
1h +IAA
Segregated
Same body
Coalescence